sures would occur through transitions[14] with $\Delta J = \pm 1$ between the lower rotational levels of OH only. At higher pressures, transitions between these lower rotational levels would become more frequent, but their effects on the distribution should be largely offset by the reduced lifetime of OH at increased pressures. This is consistent with the observation in Fig. 3 that the distribution among the lower rotational levels remained relatively cold as the pressure was increased. On the other hand, increased translational temperatures at higher pressures would tend to allow more efficient exchange of energy between the translation of H_2O and the rotation of OH in higher-lying rotational levels, thus increasing the population in these higher-lying rotational levels. Deviations from a thermalized distribution would then result if OH-OH collisions no longer remained dominant throughout the occupied rotational levels. While the effect of temperature inhomogeneity cannot be ruled out completely in our experiments with the dc discharge, this process noted above should at least be partly responsible for the deviations observed in Fig. 3. Further experiments are currently underway to elucidate this process; and the results will be published separately.

This work was supported in part by National Aeronautics and Space Administration Ames Research Center under contract number NAS2-8797, and by the Atmospheric Sciences Section, National Science Foundation.

[1]K. M. Evenson, J. S. Wells, and H. E. Radford, Phys. Rev. Lett. 25, 199 (1970).
[2]J. J. ter Meulen, W. L. Meerts, G. W. M. van Mierlo, and A. Dymanus, Phys. Rev. Lett. 36, 1031 (1976).
[3]K. Suzuki and T. Tohmatsu, Planet. Space Sci. 34, 665 (1976).
[4]C. C. Wang and L. I. Davis, Phys. Rev. Lett. 32, 349 (1974); D. K. Killinger, C. C. Wang, and M. Hanabusa, Phys. Rev. A 13, 2145 (1976).
[5]C. R. Claydon, G. A. Segal, and H. S. Taylor, J. Chem. Phys. 54, 3799 (1971).
[6]C. C. Wang and L. I. Davis, Appl. Phys. Lett. 25, 34 (1974).
[7]E. Hill and J. H. Van Vleck, Phys. Rev. 32, 250 (1928); L. T. Earles, Phys. Rev. 48, 423 (1935).
[8]D. K. Killinger and C. C. Wang, Chem. Phys. Lett. (to be published).
[9]F. P. Del Greco and F. Kaufman, Disc. Faraday Soc. 33, 128 (1962).
[10]E. R. Lyman, Phys. Rev. 53, 379 (1938).
[11]G. B. Kistiakowsky and F. D. Tabbutt, J. Chem. Phys. 30, 577 (1959).
[12]R. C. M. Learner, Proc. Roy. Soc. London, Ser. A 269, 311 (1962).
[13]K. H. Welge and F. Stuhl, J. Chem. Phys. 46, 2440 (1967).
[14]H. S. W. Massey, *Electronic and Ionic Impact Phenomena* (Oxford Univ. Press, Oxford, 1971), Vol. III, Chap. 17.
[15]U. Buck, F. Huisken, J. Schleusener, and H. Pauly, Phys. Rev. Lett. 38, 680 (1977).

Self-Steepening of the Density Profile of a CO_2-Laser-Produced Plasma

R. Fedosejevs,[a] I. V. Tomov, N. H. Burnett, G. D. Enright, and M. C. Richardson
Division of Physics, National Research Council of Canada, Ottawa, Ontario K1A 0R6, Canada
(Received 25 May 1977)

Interferometric measurements of plasmas produced by CO_2-laser pulses at intensities of 10^{14} W cm^{-2} provide direct evidence for density-profile modification due to radiation pressure.

The application of CO_2 lasers to laser fusion has long suffered from the argument that the longer-wavelength (10.6 μm) radiation of these lasers will be absorbed at plasma densities ($\sim 10^{19}$ cm^{-3}) far removed from the ablation surface. However, this view is altered if the effects of ponderomotive forces[1] in the absorption region are considered. The importance of light pressure in creating gross modification of the plasma density profile, first recognized by Kidder,[2] has recently received considerable attention,[3,4] and its effects demonstrated in computer simulation experiments[5-7] of laser-light absorption. Moreover in the regime where the radiation pressure is much greater than the local plasma pressure ($>10^{14}$ W cm^{-2} for CO_2 lasers and $>10^{16}$ W cm^{-2} for Nd:glass lasers), the abosrption should occur at a sharp density discontinuity, the position and shape of which is largely independent of wavelength.[8] In this Letter, we report the first direct measurements made of the self-steepening of the density profile of a laser-produced plasma, through the

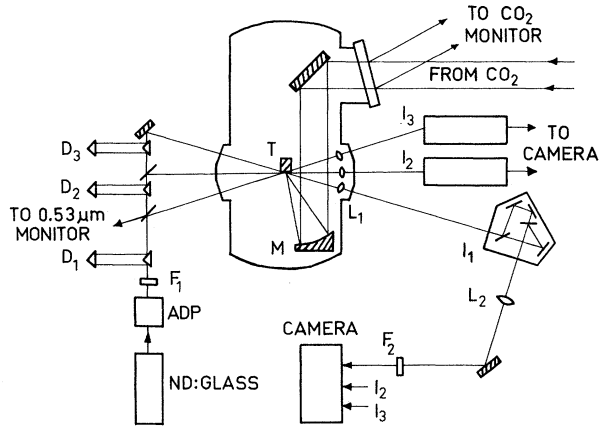

FIG. 1. Schematic diagram of the multichannel interferometer and CO_2-laser target chamber. ADP denotes the ammonium dihydrogen phosphate crystal; D_1, D_2, and D_3, double-prism beam-delay lines; F_1, 1.06-μm blocking filter; F_2, 0.53-μm, 10-Å interference filter; I_1, I_2, and I_3, folded-wavefront interferometers; L_1 and L_2, imaging lenses; M, 20-cm–focal–length off-axis parabolic mirror; T, solid target.

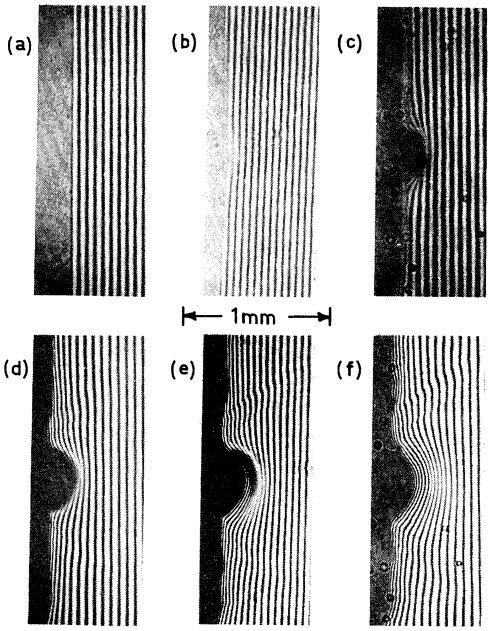

FIG. 2. Interferograms of the plasma produced on a solid aluminum target by a 30-J CO_2-laser pulse incident from the right. Frames (a)–(c) are taken during one laser shot at times $t = -1.0$, 0.6, and 1.9 ns, respectively. Frames (d)–(f) are taken on a second shot at times $t = 3.2$, 4.8, and 6.1 ns, respectively.

use of picosecond, multichannel interferometry.

The experimental system is shown schematically in Fig. 1. Plasmas were produced off planar solid targets by the output of one channel of the COCO-II short-pulse laser system,[9] producing energies of up to 60 J in a 1–2–ns(full width at half-maximum) pulse in a nearly diffraction-limited 80-mm-diam beam. The p-polarized beam was focused by a 20-cm–focal–length off-axis parabolic mirror onto targets oriented at ~20° to the optic axis, the measured focal-spot diameter of 150 μm being limited by mirror imperfections. An actively mode-locked Nd:glass laser[10] produced a single 200-ps–duration 1.06-μm pulse of energy ~1.5 mJ synchronized to the 1-ns 10.6-μm pulse to within 400 ps. After being up-converted to 0.53 μm, this pulse was split into three independently delayed beams which probed the target zone at intervals of ~1.5 ns. All three beams passed through the plasma region in the plane of the target surface but are angularly separated by 5.7°. Each beam then passed through a separate folded-wavefront interferometer[11] and was imaged onto film (Kodak plus-X) through a 10-Å interference filter. The imaging system has an aperture of $f/15$ with a measured resolution of 15 μm and was focused to within 100 μm of the center of the plasma. Precise measurements of the time, t, between the probe pulse and the 10% leading edge of the CO_2-laser pulse were obtained from the fast infrared and visible detector-oscilloscope monitoring systems having a combined resolution of ±200 ps. The shape of the CO_2-laser pulse was non-Gaussian, with a fast-detector–limited (<700 ps) leading edge and a falloff approximately of the form $\exp(-t'/\tau)$, where $\tau = 0.9$ ns.

Two triple sequences of interferograms for two shots on planar Al targets are shown in Fig. 2. The pulse energy on each shot was 30 J producing a peak power density in the focal region of $\sim 10^{14}$ W cm^{-2}. The first three interferograms show the plasma at times of $t = -1.0$, 0.6, and 1.9 ns, and the next three interferograms show the plasma at times of $t = 3.2$, 4.8, and 6.1 ns. Although in each case a small prepulse, <3 mJ, was incident on the target 25 ns earlier, there is no plasma $> 5\times10^{17}$ cm^{-3} on the target surface immediately prior to the main pulse at $t = -1.0$ ns. Before the peak of the laser pulse ($t = 0.6$ ns) the plasma appears as a blurred region on the interferogram expanding at a velocity of 10^7 cm/s, with a slight fringe shift visible. At later times the plasma expands towards the incoming laser beam within the focal zone, and in addition plasma is observed on a large surrounding surface region up to 1.5 mm from the focal point. The

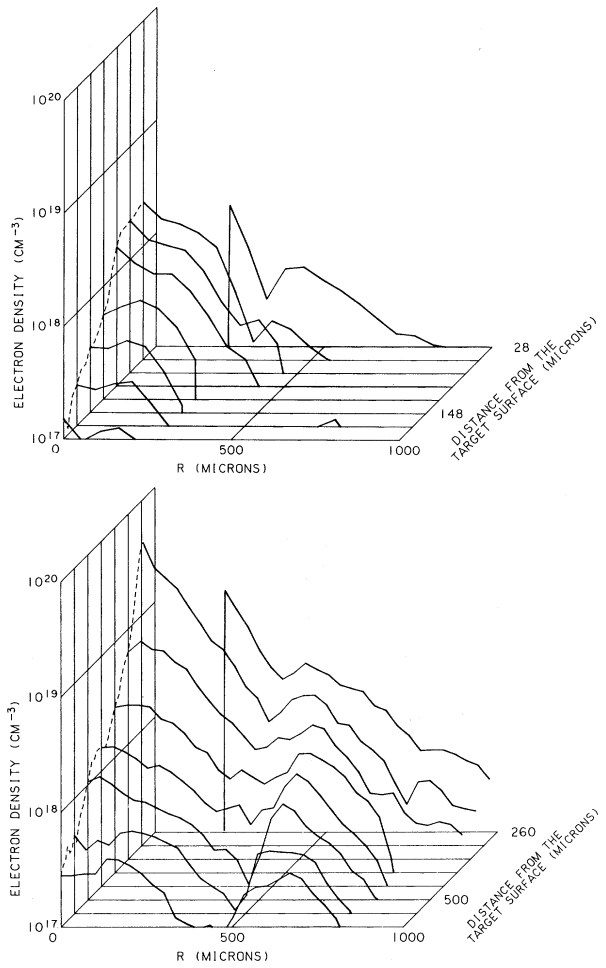

FIG. 3. Radial electron-density distribution of the plasma produced on a solid aluminum target by a 30-J CO_2-laser pulse at times (a) 0.6 ns and (b) 3.2 ns. The electron density is plotted vs radial distance from the laser axis at various distances from the original target surface which is at the rear of each plot.

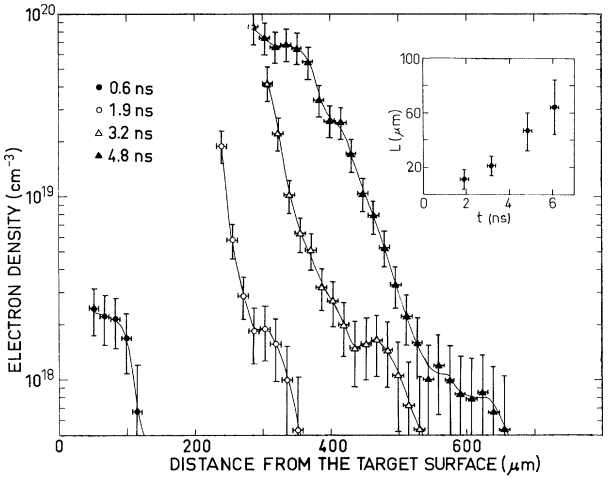

FIG. 4. Plot of axial electron density vs distance from the original target surface at various times. The inset shows the scale length $L = n_e (dn_e/dx)^{-1}$ in the region of the critical density surface at various times relative to the leading edge of the CO_2-laser pulse.

bulk of the plasma remains cut off from view, but as the expansion slows down and the density gradient decreases, fringe shifts are observable further into the leading edge of the plasma.

In order to compute the corresponding electron density profiles the fringe positions on the above interferograms were measured and digitized. With assumption of cylindrical symmetry around the central axis of the expanding plasma, the electron densities were calculated at various distances from the target surface with use of a 40- or 20-point, piecewise-cubic–polynomial, Abel inversion. Two of the resultant radial electron-density profiles from the interferograms of Fig. 2, at times $t = 0.6$ and $t = 3.2$ ns are shown in Fig. 3. The plasma center is at the left, and the target surface is at the back of each plot. The distances are given from the original target surface, but the electron densities are only displayed up to where the fringes start to be cut off by the dense-plasma region, indicated by a straight line to the axis. At $t = 0.6$ ns [Fig. 3(a)], the only visible feature is a shelf at $\sim 2\times10^{18}$ cm^{-3} extending ~ 40 μm from the front of the main body of the plasma. At the later time $t = 3.2$ ns, the full density profile through the critical region is observable together with a shock-wave–like structure propagating radially outwards into the low-density plasma region. This structure shows up as wings in the density profiles and is clearly visible in the later-time interferograms.

The axial density profiles for four of the interferograms in Fig. 2 are shown in Fig. 4. The error in the electron density measurement is a combination of an absolute error of $\pm 5\times10^{17}$ cm^{-3} due to the limit in accuracy of fringe-position measurement, and an additional error of $\pm 20\%$ due to point-to-point variations in the data along one inversion line. During the laser pulse, the axial profiles indicate the existence of a shelf in the leading edge of the plasma at a density in the region of 2×10^{18} cm^{-3}. At 1.9 ns, the critical density ($n_c = 10^{19}$ cm^{-3}) surface becomes visible and the scale length $L = n_e(dn_e/dx)^{-1}$ at n_c can be determined. This scale length increases with time from a value of 11 μm at 1.9 ns and is plotted as a function of time in the inset in Fig. 4.

At 4.8 ns, an upper shelf structure is observed with a density of 7×10^{19} cm^{-3}.

The above results showing a steep rise through the critical density, together with some evidence for the existence of an upper density plateau, can be understood by considering the effects of radiation pressure. The ratio of incident radiation pressure to kinetic pressure at the critical density surface is given by $r_p = I/cn_c T_e = \frac{1}{2}(v_0/v_e)^2$, where v_0 is the electron quiver velocity, and v_e the electron thermal velocity. In the present case for peak intensities of $I = 10^{14}$ W cm^{-2} and measured electron temperatures of $T_e = 400$ eV,[12] the pressure ratio would be $r_p = 5.2$. Simulation results[5-7] mainly at weaker pressure ratios ($r_p \lesssim 1$) predict the formation of upper and lower density shelves joined by a very steep rise through the critical density region with a scale length of the order of 20 Debye lengths. In the present experiment, the scale length at the peak of the laser pulse was beyond the resolution of the interferometric system, which indicates that its value was less than or equal to 11 μm, measured at 1.9 ns. Such a steep rise through the critical density region is much shorter than would be predicted for a freely expanding isothermal plasma. Simple balancing of radiation pressure and plasma pressure would predict an upper shelf density of $5n_c$ but this could be further enhanced by momentum deposition from particles accelerated out of the critical density region away from the plasma. The late-time decaying plasma profile indicates such an upper shelf structure with a density of $7n_c$. This is consistent with x-ray measurements[12] which indicate the source of thermal x rays is from a region of density 10^{20} cm^{-3} or greater. The observation of a steep density profile through the quarter critical region is compatible with measurements of CO_2-laser light backscatter[13] which indicate reduced $\frac{3}{2}\omega_0$ generation compared to experiments at 1.06 μm. In the axial profiles illustrated, and in results from other similar shots a lower density shelf structure at about between $0.2n_c$ and $0.5n_c$ is seen in the expanding front of the plasma during the CO_2-laser pulse. This structure which is higher in density than the supersonic lower shelf predicted by one-dimensional models[3] and lower in density than the subcritical plateau predicted by steady-state spherical models[4] is suggestive of a density perturbation due to a standing-wave pattern in the incoming radiation.

The observation of a steep density profile with a scale length on the order of λ_0 will have implications in determining the relative importance of various absorption mechanisms such as resonant absorption, parametric-decay instabilities, and others. These results indicate that radiation pressure is a dominating factor in determining the density profile, and if this remains true at higher irradiance levels, then the plasma profile should largely be governed by the incident intensity rather than the wavelength of the laser radiation.

The authors wish to acknowledge the continuing excellent technical support of P. Burtyn, G. A. Berry, and W. J. Orr.

---

[a]Work performed in partial fulfillment of a Ph.D. degree, University of Toronto, Toronto, Canada.

[1]H. Hora, D. Pfirsch, and A. Schlüter, Z. Naturforsch. 22A, 278 (1967).

[2]R. E. Kidder, in *Proceedings of Japan-U.S. Seminar on Laser Interaction with Matter*, edited by C. Yamanaka (Tokyo International Book Co., Tokyo, 1975), p. 331.

[3]K. Lee, D. W. Forslund, J. M. Kindel, and E. L. Lindman, Phys. Fluids 20, 51 (1977).

[4]P. Mulser and C. van Kessel, Phys. Rev. Lett. 38, 902 (1977).

[5]D. W. Forslund, J. M. Kindel, K. Lee, E. L. Lindman, and R. L. Morse, Phys. Rev. A 11, 679, (1975); D. W. Forslund, J. M. Kindel, K. Lee, and E. L. Lindman, Phys. Rev. Lett. 36, 35 (1976).

[6]J. S. DeGroot and J. E. Tull, Phys. Fluids 18, 672 (1975).

[7]K. G. Estabrook, E. J. Valeo, and W. L. Kruer, Phys. Fluids 18, 1151 (1975).

[8]B. Bezzerides, D. F. DuBois, D. W. Forslund, J. M. Kindel, K. Lee, and E. L. Lindman, in *Proceedings of the Sixth International Conference on Plasma Physics and Controlled Nuclear Fusion, Berchtesgaden, West Germany, 1976* (International Atomic Energy Agency, Vienna, 1977).

[9]M. C. Richardson, N. H. Burnett, H. A. Baldis, G. D. Enright, R. Fedosejevs, N. R. Isenor, and I. V. Tomov, in Proceedings of the Fourth Workshop on Laser Interaction and Related Plasma Phenomena, Troy, New York, November 1976 (to be published).

[10]I. V. Tomov, R. Fedosejevs, M. C. Richardson, and W. J. Orr, Appl. Phys. Lett. 29, 193 (1976); I. V. Tomov, R. Fedosejevs, and M. C. Richardson, Appl. Phys. Lett. 30, 164 (1977).

[11]R. Fedosejevs, I. V. Tomov, N. H. Burnett, and M. C. Richardson, in Proceedings of the Twelfth International Conference on High Speed Photography, Toronto, Canada, August 1976 (to be published).

[12]G. D. Enright, N. H. Burnett, and M. C. Richardson, Appl. Phys. Lett. 31, 494 (1977).

[13]N. H. Burnett, H. A. Baldis, M. C. Richardson, and G. D. Enright, Appl. Phys. Lett. 31, 172 (1977).

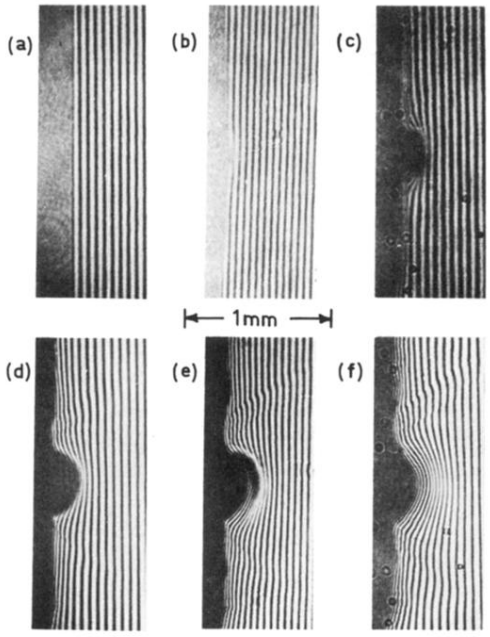

FIG. 2. Interferograms of the plasma produced on a solid aluminum target by a 30-J CO_2-laser pulse incident from the right. Frames (a)–(c) are taken during one laser shot at times $t = -1.0$, 0.6, and 1.9 ns, respectively. Frames (d)–(f) are taken on a second shot at times $t = 3.2$, 4.8, and 6.1 ns, respectively.